Proceedings of 2016 IEEE
International Conference on Mechatronics and Automation
August 7 - 10, Harbin, China

High-Resolution Cell Manipulation for Longstanding Load on Red Blood Cells

Chia-Hung Dylan Tsai, Mitsuhiro Horade,
Hiroaki Ito and Makoto Kaneko
Dept. of Mechanical Engineering
Osaka University, Suita, Japan
{*tsai@hh., horade@, ito@hh., mk@*}
mech.eng.osaka-u.ac.jp

Motomu Tanaka

iCeMS, Kyoto University, Japan
Inst. for Physical Chemistry
University of Heidelberg, Germany
tanaka@uni-heidelberg.de

***Abstract*— A high-resolution cell manipulation system is presented for investigating red blood cell deformation under longstanding load in this paper. Because the low Reynolds number in microfluidic system, cell position can be manipulated by controlling the flow in a microchannel. A high-speed vision system is embedded in the system for providing cell present position as the feedback signal for the controller while a syringe pump actuated by a piezoelectric actuator is employed for flow control in the channel. The system is utilized for applying longstanding load on human red blood cells. The longstanding load is generated by manipulating a cell into a constriction channel where the cross-sectional size is smaller than the size of the cell. The cell has to deform due to the geometrical constraints of the constriction. Both the system performance and cell response to longstanding load have been evaluated. The manipulation system successfully achieves cell positioning as accurate as $0.24\mu m$ while red blood cells are found always exponentially shrink with respect to time, and an average shrinkage of $1.82\mu m$ in 5 minutes is observed. Details of system construction and discussion on the cell response are presented.**

***Index Terms*— microfluidics, red blood cell, longstanding load**

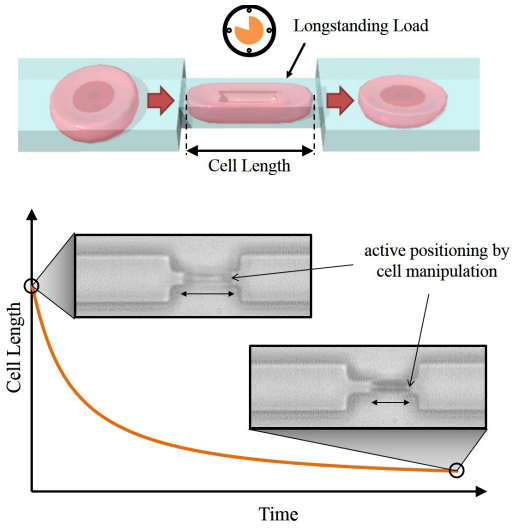

Fig. 1. Continuous deformation of RBCs under longstanding load is experimentally observed.

I. Introduction

Microfluidic system provides an very useful platform for evaluating cell mechanics, and has become popular in recent years [1]. For example, Hirose *et al.* put cells through a narrow throat in a microfluidic system, and determine the cell stiffness based on the transit time [2]. Sugiura *et al.* measure mechanical characteristics of single cells by moire fringe [3]. Two of the advantages of microfluidic system are cleanness and simpleness. The cleanness is because that the microfluidic system is a closed environment, except inlets and outlets. Therefore, cell operations can be performed from direct contact with air or surrounding space, and as a result, the chance of contamination is greatly reduced. The simpleness is due to the low Reynolds number, so the flow inside the channel is mostly laminar, except the cases with hundreds micron wide channels [4]. Cells, or any suspending micro object, are simply moved along parallel streamlines, which makes the flow-based manipulation becomes possible [5]. In this paper, we focus on such a flow-based cell manipulation and examine cell behavior under longstanding load.

Figure 1 illustrates an overview of cell manipulation and observed cell response under longstanding load. The top of Fig. 1 shows the manipulation sequence where a target cell is firstly captured in front of a narrow channel before the test. The cell is then moved into the constriction channel by the flow-based manipulation. Due to the geometrical constraints of the constriction, the cell has to deform for entering the constriction, and as a result, a load is applied to the cell from the channel walls. After keeping the cell inside the constriction for a specified duration, the cell is manipulated to the wide part of the channel from the constriction. The same test is continuously applied on different cells for determine general cell response under longstanding load.

The lower half of Fig. 1 illustrates what we have observed in the test as cell length getting shorter and shorter with time. Two example cell images before and after longstanding load are demonstrated. Vision system is implemented in the manipulation system for keeping cell position inside the narrow channel as well as monitoring cells' responses. Such a time-dependent deformation demonstrates a viscoelastic property of

978-1-5090-2396-7/16/$31.00 ©2016 IEEE

cells. If the cell is pure elastic material, the deformation should be concluded as soon as it is moved into the constriction. However, the cell slowly deforms for reaching another equilibrium state. The rate of deformation under such a longstanding load represents cell mechanics, and could be a new index for cell evaluation.

Human red blood cells (RBCs) have been employed for the longstanding load test in this work. All the tested cells exhibit similar deformation pattern that cell length, in the direction parallel to the channel, exponentially decreased with time, and tries to reach asymptotic values. The cell length is measured by computer image processing from captured image frames. The experimental results show an average shrinkage of $1.82\mu m$ among all tested cells.

The rest of this paper is organized as follows: After a brief review of the related work in Section II, the cell manipulation system and experimental details are introduced in Section III. Experimental results on RBCs from a healthy subject are presented in Section IV. The experimental results is discussed in Section V. Finally, the paper is concluded in Section VI.

II. Related Works

There are different approaches for manipulating cells [6]. These methods can be categorized based on the nature of manipulation as direct contact method [7][8], flow-based method [9][5], optical method [10][11], electrical method [12], magnetic methods[13][14], and acoustic method. [15][16]. For example, Sakuma *et al.* applied cell manipulation to a cell for fatigue evaluation by continuous moving through a narrow channel [17]. While biological cells are usually considered as viscoelastic material and exhibit time dependent property such as stress relaxation and strain creep [18], there are medical researches showing direct or indirect relations between cell characteristics and diseases [19]. For example, Lim *et al.* found that RBCs tend to be more stiff from a subject suffered from Malaria [20].

Microfluidic system has been used as a test platform for deformability evaluation on human RBCs in our former works [21][22][23][24]. To the best of the authors' knowledge, this work is the first work focus on the deformation of red blood cell under longstanding load using a microfluidic channel.

III. Experimental System

A. Evaluation Method

Figure 2 illustrates an overview of how the longstanding load is applied to a cell using microfluidic system. Figure 2(a) and (b) are conceptual and practical images of the test, respectively. A target cell is first allocated in the test platform as the grippers *catch* the cell in Fig. 2(a). The next step is to applied the load by compressing the cell.

However, the size of a RBC is usually between $6\mu m$ to $8\mu m$ in diameter. It is too small to be directly manipulated by micro grippers, such as the one illustrated in Fig. 2(a), and it is also difficult to provide a stable displacement to deform the cell within few micrometers for a long time. Therefore, a practical

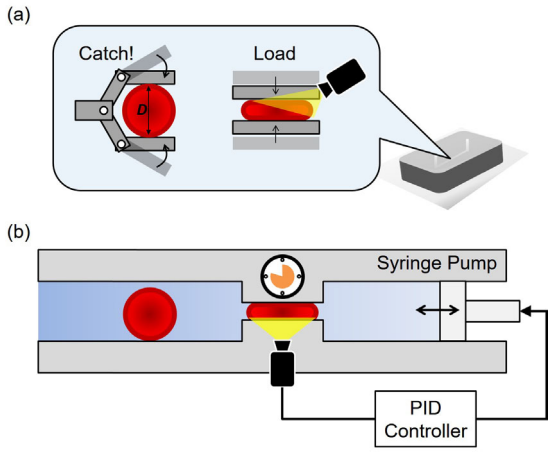

Fig. 2. An overview of the evaluation system. (a) A conceptual image of the constructed system for the evaluation. (b) On-chip cell manipulation is utilized instead of mechanical grippers.

system using flow-based cell manipulation is employed as shown in Fig. 2(b) [25]. Instead of catch and load cell by robotic grippers, cell is manipulated in front of and inside a constriction channel, respectively. The manipulation is performed using proportional-integral-derivative (PID) feedback control with cell present position as the input and syringe pump as the output. A target position is given to the controller and cell is manipulated by the flow generated from the syringe pump. For example, in order to move a cell from the left of the constriction to the inside of constriction as shown in Fig. 2(b), the piston on the right of Fig. 2(b), which represents a syringe pump, will move to the right. A fluid flow from left to right will then be generated inside the microchannel because the pressure on the right reduces as a result of the piston movement. Due to the low Reynolds number in a microfluidic channel (usually smaller than one) a cell suspended in the fluid moves with fluid. Once the cell reaches to the target position, the piston will push back for stopping the flow, and the manipulation is completed.

B. Experimental Setup and Chip Fabrication

Figure 3 shows a photo of the actual experimental setup where the system is constructed by a microfluidic chip, a high-speed camera, a microscope, a syringe pump and a piezoelectric actuator. A snapshot with scale is shown on the top of Fig. 3, and the channel width is $10\mu m$ and $3.5\mu m$ for the wide part and constriction part, respectively. The height of the channel is $3.5\mu m$ in the entire microfluidic device. The combination of microscope and high-speed camera provides high-speed vision signal for cell position feedback while the piezoelectric actuator and syringe pump generate fluid flow inside the microfluidic chip to move the cell.

Figure 4(a) to (h) shows a step-by-step process of making the microfluidic chip. Firstly, a thin layer of negative photoresist (SU8) is coated on the surface of a clean silicon substrate as shown in Fig. 4(a) and (b). The thickness of

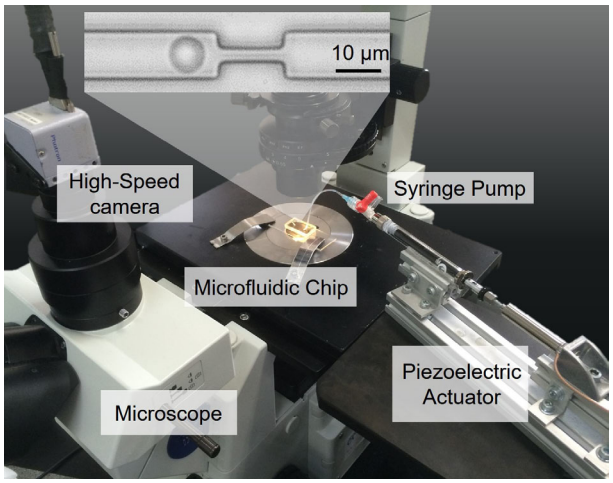

Fig. 3. A photo of actual experimental system.

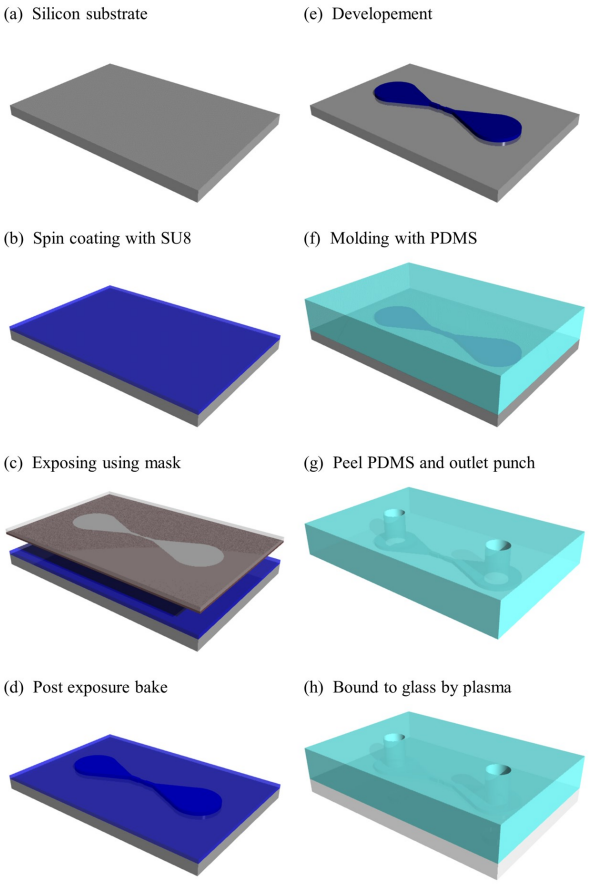

Fig. 4. The fabrication process for making the microfluidic test platform. (a) Silicon substrate is used as the mold base. (b) Negative photoresist SU8 is spin coated on the surface of the substrate. (c) The photoresist is exposed to light with a mask with channel pattern. (d) Exposed mold is bake for cure. (e) The unexposed part is washed out during development and the mold is fabricated. (f) PDMS is poured on the top of the mold for molding. (g) channel pattern is molded on the PDMS and two outlets are punched for tubing. (h) The PDMS chip is bounded to a glass substrate and the chip fabrication is completed.

the coating determines the height of the microchannel. The negative photoresist is exposed to light patterned by a mask with channel pattern on it as shown in Fig. 4(c), and then the whole substrate is baked for 30 minutes shown in Fig. 4(d) as the post process of the exposure. The part exposed to the light turned to be solid and stable, which makes it remains on the substrate after rinsing with development chemicals as shown in Fig. 4(e). Fig. 4(a) to (e) is the process of making a master mold for the chip. From Fig. 4(f) to (h), a microfluidic chip is fabricated from the mold. Polydimethylsiloxane (PDMS) is a material commonly used for microfluidic system because of its properties of being stable and transparent. PDMS is poured on the top of the mold and bake for cure as shown in Fig. 4(f). One inlet and one outlet holes are punched after the PDMS is cured as in Fig. 4(g). Finally, the PDMS chip is securely bounded to a glass substrate using plasma treatment on both the bounding surfaces.

C. Experimental Procedure

The experiments were performed under the following processes:

- **Cell sample preparation**
  RBCs from a healthy subject are utilized for the test in this paper. The volunteer cell donor has read and agreed the consent of the experiment prior to the test. A commercial disposable finger prink is used for lancing the blood from the donor. The lanced wound is immediately sterilized after a drop of blood (about $20\mu l$) is obtained. The blood is diluted with standard saline whose concentration of sodium chloride (NaCl) is 0.9%. It is because that more than five millions of RBCs are normally in a microliter of blood, and single cell evaluation is not possible without a proper dilution to reduce the number of RBCs in a unit volume. The mixed RBC sample is put on a low-speed rotator for 10 minutes for RBCs to adopt to the new osmotic condition.
- **Injection of cell sample into the microfluidic channel**
  RBC sample is injected into the microfluidic channel by place a drop of the sample at the inlet with a disposable syringe. The syringe pump is connected to the inlet after the sample placement, and the piezoelectric actuator is mounted on the syringe piston for pump control. Before the sample injection, the microfluidic channel is filled with standard saline for lubrication on the channel surface as well as for removing the air bubbles in the channel. If air bubbles exist in the flow path, the performance of the manipulation will be compromised due to the compressibility of air. The air bubbles can be removed by giving a positive fluid pressure to the channel because PDMS is air preamble so air can be directly pushed out.
- **Cell position control and control sequence**
  Three steps of control sequence is applied for this test, and they are the operations of catch, load and release. The initial fluid flow is rapid in the channel due to small cross-sectional area. The operation of catch is to

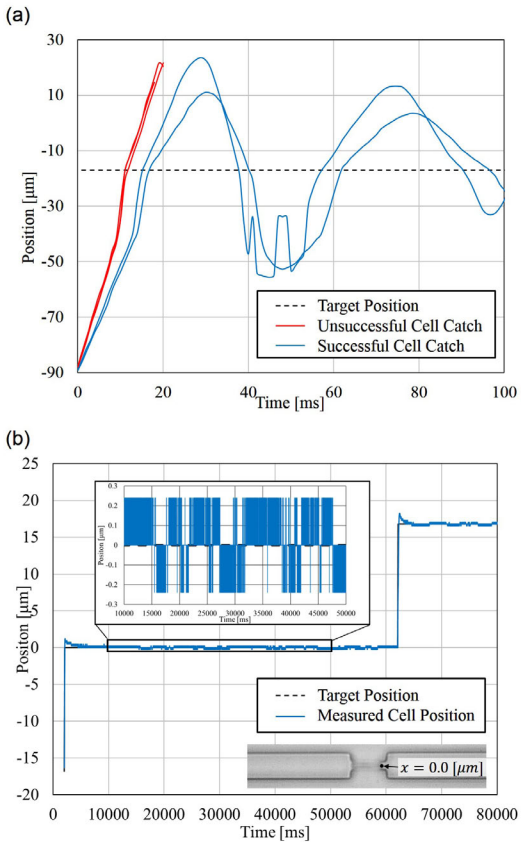

Fig. 5. The performance of cell positioning. The dash line and solid line are the given target position and the actual cell position, respectively.

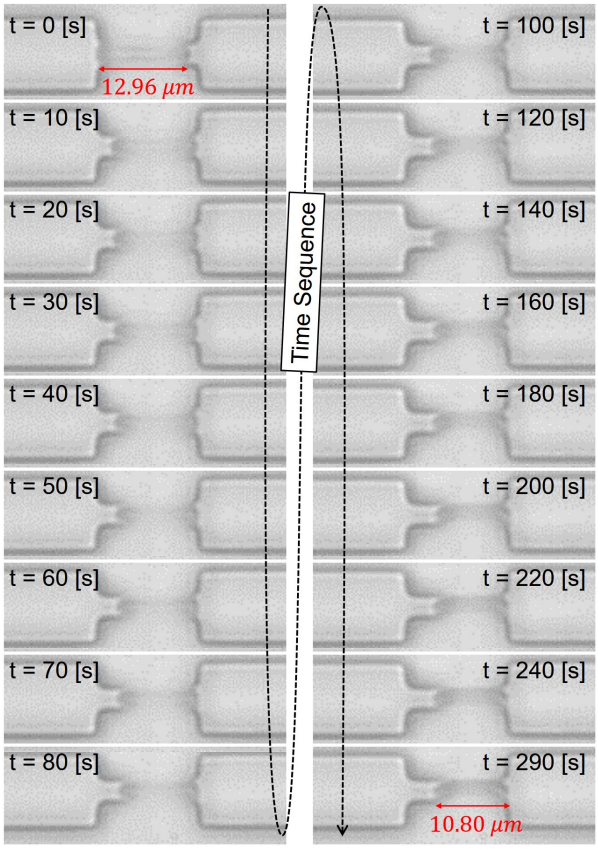

Fig. 6. Example of cell photos under longstanding load.

position a RBC in front of the constriction from the rapid flow. RBCs usually only appear on the viewable zone for few milliseconds, so high-speed camera and high-speed actuator is necessary to perform the catch. After the catch operation, the cell is moved into the constriction part for deformation. In this test, a duration of 5 minutes is specified for the load operation. RBC shape is recorded by the camera while the position is maintained in the constriction at the same time. Finally, the cell is pushed out from the constriction and a test is completed. The same test is applied on multiple RBCs and the results is shown in the following Section IV.

IV. Experimental Results

A. The performance of cell positioning

Figures 5(a) and (b) are the measured performance of cell positioning for the operations of catch and load, respectively. Successful and unsuccessful operations of catch are shown in Fig. 5(a) where the dashed line represents the target catch position. We found that the flow rate of about $5\mu m/ms$ is the limit speed for successful catch. For the cell moving faster than $5\mu m/ms$, the manipulation system couldn't response in-time to stop the cell in front of the constriction.

Figure 5(b) shows the performance of cell position during the operation of longstanding load. The blue data is the measured cell position while the dashed line, which is mostly covered by the data, is the target position. Cell position from 10s to 50s is further zoomed-in for showing the precision of the manipulation. The cell positioning is stable with the error of $\pm 0.24\mu m$. The distance of $0.24\mu m$ is equivalent to the distance of a pixel on the captured image frame. In other words, the system is able to control the cell position within one pixel.

B. Cell deformation under longstanding load

Figure 6 shows an example of time-sequenced images captured during a longstanding load. The total duration is 290 seconds, and it can be seen that the initial length of the RBC is longer than the cell length after the 290-second load. For this particular example, the cell length is changed from $12.96\mu m$ to $10.80\mu m$, which gives a total shrinkage of $2.16\mu m$. During the longstanding load, no additional load is applied to the cell except the slight flow adjustment for maintaining cell position in the constriction. In other words, the shrinkage is very possible due to the longstanding load.

Figure 7 shows the image process method for determining the cell length during the longstanding load. By utilizing the image process, we can determine the length of cell systematically and consistently from frame to frame. In other words, errors from manual measurement can be removed. The image processing include four steps as the example shown in

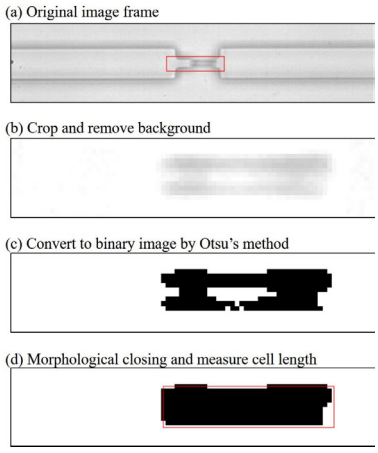

Fig. 7. Automatic image process is utilized for consistent measurement of cell length.

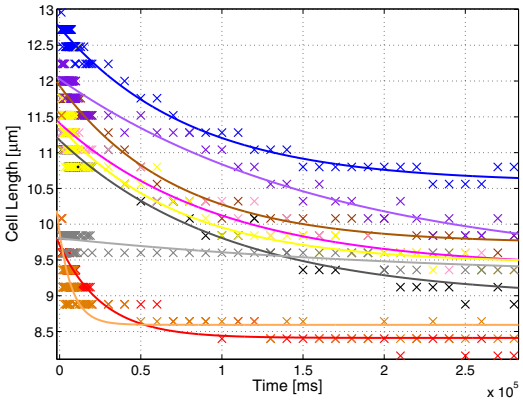

Fig. 8. Experimental results of shrinking cell length under longstanding load.

TABLE I
THE RESULTS OF CURVE FITTING

	$L(t) = ae^{-bt} + c$				
Cell#	a	b	c	R^2	SSE
1	1.3	3.7×10^{-5}	8.4	0.93	1.66
2	2.2	1.2×10^{-5}	10.6	0.98	1.21
3	2.2	1.4×10^{-5}	9.7	0.98	1.34
4	2.2	1.0×10^{-5}	9.0	0.89	5.70
5	2.0	1.0×10^{-5}	9.4	0.91	3.93
6	1.9	1.3×10^{-5}	9.5	0.83	8.60
7	1.3	12.1×10^{-5}	8.6	0.53	13.51
8	0.6	0.4×10^{-5}	9.2	0.56	1.15
9	2.7	0.6×10^{-5}	9.4	0.96	2.11
AVG	1.8	2.5×10^{-5}	9.3	0.84	4.36
STD	0.6	3.5×10^{-5}	0.61	0.16	4.01

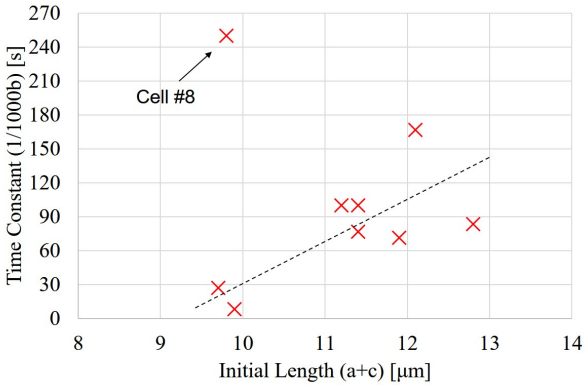

Fig. 9. The correlation between initial cell length and the time constant of shrinkage.

Figs. 7(a) to (d), respectively. The captured image is firstly cropped to only the area of interest as the red rectangle in Fig. 7(a) and applied background removal by subtracting background image, which is recorded before each test. The gray scaled cell image in Fig. 7(b) is converted to binary image as shown in Fig. 7 by Otsu's method [26]. Because the binary image is not always a clear cell, morphological closing on the black objects is applied and the cell can be reconstructed as shown in Fig. 7(d). Finally, the length of the cell is determined by the length of black object in Fig. 7(d)

Figure 8 shows the measurement results from the experiment. The crosses marks represent each length measurement while the solid curves show the least-square fit for each data set. A total of 9 RBCs were tested, and all RBCs shrank during the longstanding load in the test. According to the tendency of the length change, an exponential function is employed for curve fitting as

$$L = ae^{-bt} + c \tag{1}$$

where L and t are the cell length in micrometer, time in millisecond while a, b and c are the coefficients to be determined by the fit. The coefficients a, b and c also represent the physical meaning of total amount of length change to a new equilibrium, the inverse of time constant of the change and the predicted equilibrium length of the change, respectively.

Table I is the list of fit results on measured cell length and the goodness of the fit as coefficient of determination R^2 and sum of squared error (SSE). The average of R^2 value is 0.84 which shows a fair fit. The cell length change in 290 seconds is ranged from $0.6\mu m$ to $2.7\mu m$ with an average of $1.8\mu m$. The time constant can be determined by $1/b$ which gives an average time constant of 98.2 seconds.

Figure 9 shows the correlation between cell initial length versus determined time constants. A positive correlation of 0.71 is found if not considering outlier of Cell#8. It shows that a bigger cell tends to shrink slower based on the analysis results.

V. DISCUSSION

Figure 10 illustrates a possible interpretation of why the cell continuously deform during the longstanding load. The cross-sectional area of the microchannel used in the experiments is rectangular, and there are gaps at the corners when the RBCs are deformed in the constriction. The RBCs may try to fit

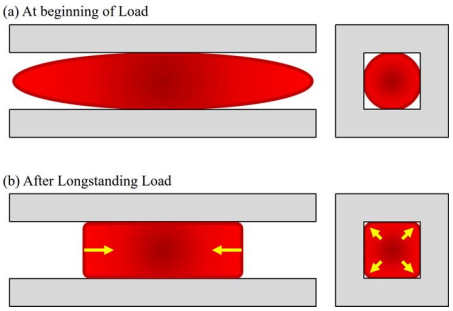

Fig. 10. Cells gradually adopt to the rectangular shape of channel. (a) The cell shape is initially elliptical when it just entered the constriction channel. (b) The cell shape gradually deform to fit the rectangular shape after longstanding load, and as a result the cell length becomes shorter.

the gaps by expanding its volume in the cross-sectional area, which leads to the shrinkage of length assuming constant surface area of a RBC. Although the interpretation is reasonable, it needs to be further verified by implementing vision system from the side view.

VI. Concluding Remarks

A high-resolution cell manipulation system is developed for the evaluation of cell deformability under longstanding load. By positioning RBCs inside a microfluidic constriction channel, continuous deformation of RBC is experimentally observed and presented in this paper. Two concluding remarks are as follows:

- The performance of the test system is confirmed. The resolution of cell positioning is as accurate as 240 nanometer.
- RBCs are found consistently shrinking in length under longstanding load. The time constant of the shrinkage is 98.2 seconds, and the average shrinking length is $1.82\mu m$.

VII. Acknowledgment

We would like to specially thank Mr. Ryo Murakami for his assistance in experiments. This work is partially supported by JSPS KAKENHI Grant #15H05761, #26820086 and #16K18051.

References

[1] Y. Zheng, J. Nguyen, Y. Wei, and Y. Sun. Recent advances in microfluidic techniques for single-cell biophysical characterization. *Lab on a chip*, 13(13):2464–2483, 2013.

[2] Y. Hirose, K. Tadakuma, M. Higashimori, T. Arai, M. Kaneko, R. Iitsuka, Y. Yamanishi, and F. Arai. A new stiffness evaluation toward high speed cell sorter. In *Proc. of the IEEE Int. Conf. on Robotics and Automation, ICRA*, pages 4113–4118, Anchorage, USA, May 2010.

[3] Hirotaka Sugiura, Shinya Sakuma, Makoto Kaneko, and Fumihito Arai. On-chip method to measure mechanical characteristics of a single cell by using moir fringe. *Micromachines*, 6(6):660–673, 2015.

[4] D. Di Carlo, D. Irimia, R. G. Tompkins, and M. Toner. Continuous inertial focusing, ordering, and separation of particles in microchannels. *Proc. of the National Academy of Sciences, PNAS*, 104(48):18892–18897, 2007.

[5] T. Monzawa, M. Kaneko, C. D. Tsai, S. Sakuma, and F. Arai. On-chip actuation transmitter for enhancing the dynamic response of cell manipulation using a macro-scale pump. *Biomicrofluidics*, 9:014114, 2015.

[6] Hoyoung Yun, Kisoo Kim, and Won Gu Lee. Cell manipulation in microfluidics. *Biofabrication*, 5(2):022001, jun 2013.

[7] Ebubekir Avci, Kenichi Ohara, Chanh Nghiem Nguyen, Chayooth Theeravithayangkura, Masaru Kojima, Tamio Tanikawa, Yasushi Mae, and Tatsuo Arai. High-speed automated manipulation of microobjects using a two-fingered microhand. *IEEE Transactions on Industrial Electronics*, 62(2):1070–1079, 2015.

[8] N. Chronis and L. P. Lee. Electrothermally activated su-8 microgripper for single cell manipulation in solution. *Journal of Microelectromechanical Systems*, 14(4):857 – 863, 2005.

[9] S. Sakuma, K. Kuroda, F. Arai, T. Taniguchi, T. Ohtani, Y. Sakata, and M. Kaneko. High resolution cell positioning based on a flow reduction mechanism for enhancing deformability mapping. *Micromachines*, 5(4):1188–1201, 2014.

[10] Y. Tan, D. Sun, J. Wang, and W. Huang. Mechanical characterization of human red blood cells under different osmotic conditions by robotic manipulation with optical tweezers. *IEEE Transactions on Biomedical Engineering*, 57(7):1816–1825, 2010.

[11] Hu Zhang and Kuo-Kang Liu. Optical tweezers for single cells. *Journal of the Royal Society, Interface / the Royal Society*, 5(24):671–690, jul 2008.

[12] Joel Voldman. Electrical forces for microscale cell manipulation. *Annual Review of Biomedical Engineering*, 8:425–454, 2006.

[13] M. Hagiwara, T. Kawahara, Y. Yamanishi, T. Masuda, L. Feng, and F. Arai. On-chip magnetically actuated robot with ultrasonic vibration for single cell manipulations. *Lab on a Chip*, 11:2049, 2011.

[14] Benjamin D Matthews, Darryl R Overby, Francis J Alenghat, John Karavitis, Yasuchi Numaguchi, Philip G Allen, and Donald E Ingber. Mechanical properties of individual focal adhesions probed with a magnetic microneedle. *Biochemical and Biophysical Research Communications*, 313(3):758–764, jan 2004.

[15] Zhangming Mao, Yuliang Xie, Feng Guo, Liqiang Ren, Po-Hsun Huang, Yuchao Chen, Joseph Rufo, Francesco Costanzo, and Tony Jun Huang. Experimental and numerical studies on standing surface acoustic wave microfluidics. *Lab on a chip*, pages 515–524, 2015.

[16] J Dual and D Moller. Acoustofluidics 04: Piezoelectricity and application in the excitation of acoustic fields for ultrasonic particle manipulation. *Lab Chip*, 12(3):506–514, 2012.

[17] S. Sakuma, K. Kuroda, C. D. Tsai, W. Fukui, F. Arai, and M. Kaneko. Red blood cell fatigue evaluation based on close-encountering point between extensibility and recoverability. *Lab On A Chip*, 14(6):1135–1141, 2014.

[18] Y. C. Fung. *Biomechanics: Mechanical Properties of Living Tissues*. Springer-Verlag, 1993.

[19] FC F. C. Mokken, M. Kedaria, and C. P. Henny. The clinical importance of erythrocyte deformability, a hemorrheological parameter. *Annals of Hematology*, 64:113–122, 1992.

[20] C. T. Lim. Single cell mechanics study of the human disease malaria. *Journal of Biomechanical Science and Engineering*, 1(1):82–92, 2006.

[21] C. D. Tsai, S. Sakuma, F. Arai, and M. Kaneko. A new dimensionless index for evaluating cell stiffness-based deformability in microchannel. *IEEE Transactions on Biomedical Engineering*, 61(4):1187–1195, 2014.

[22] C. D. Tsai, K. Mizoue, M. Kaneko, S. Sakuma, and F. Arai. Novel microfluidic chip for extracting cell deformability. In *Proc. IEEE Int. Conf. on Mechatronics and Automation*, pages 2136–2144, Beijing, China, August 2015.

[23] C. D. Tsai, M. Kaneko, S. Sakuma, and F. Arai. Phase decomposition of a cell passing through a μ-channel - a method for improving the evaluation of cell stiffness. In *Proc. IEEE Int. Conf. on Mechatronics and Automation*, pages 138–143, Chengdu, China, August 5-8 2012.

[24] C. D. Tsai, S. Sakuma, F. Arai, T. Taniguchi, T. Ohtani, Y. Sakata, and M. Kaneko. Geometrical alignment for improving cell evaluation in a microchannel with application on multiple myeloma red blood cells. *RSC Advances*, 4(85):45050–45058, 2014.

[25] R. Murakami, C. D. Tsai, H. Ito, M. Tanaka, S. Sakuma, F. Arai, and M. Kaneko. Catch , load and launch toward on-chip active cell evaluation. In *Proc. of the IEEE Int. Conf. on Robotics and Automation, ICRA*, pages 1713–1718, Stockholm, Sweden, May 2016.

[26] N. Otsu. A threshold selection method from gray-level histograms. *IEEE Transaction on System, Man, and Cybernetics*, 9(1):62–66, 1979.